Kinetic Characterization of Thiolate Anion Formation and Chemical Catalysis of Activated Microsomal Glutathione Transferase 1†

Richard Svensson,‡ Johan Alander,‡ Richard N. Armstrong,§ and Ralf Morgenstern*,‡

Institute of Environmental Medicine, Division of Biochemical Toxicology, Karolinska Institutet, Box 210, 17177 Stockholm, Sweden, and Department of Biochemistry, Vanderbilt University School of Medicine, Nashville, Tennessee 37232-0146

Received April 15, 2004; Revised Manuscript Received May 7, 2004

ABSTRACT: Microsomal glutathione transferase 1 (MGST1) displays the unique ability to be activated, up to 30-fold, by the reaction with sulfhydryl reagents, e.g., *N*-ethylmaleimide. Analysis of glutathione (GSH) thiolate formation, which occurs upon mixing activated MGST1 with GSH, reveals biphasic kinetics, where the rapid phase dominated at higher GSH concentrations. The kinetic behavior suggests a two-step mechanism consisting of a rapid GSH-binding step ($K_D^{GSH} \approx 10$ mM), followed by slower formation of thiolate ($k_2 \approx 10$ s^{-1}). The release rate (or protonation of the enzyme GSH thiolate complex) of GS$^-$ was slow ($k_{-2} = 0.016$ s^{-1}), consistent with overall tight binding of GSH. Electrophilic second substrates react rapidly with the E•GS$^-$ complex, and again, a two-step mechanism is suggested. In comparison to the unactivated enzyme [Morgenstern et al. (2001) *Biochemistry 40*, 3378−3384], the mechanisms of GSH thiolate formation and electrophile interaction are similar; however, thiolate anion formation is enhanced 30-fold in the activated enzyme, contributing to an increased k_{cat} (3.6 s^{-1}). Interestingly, in the activated enzyme, thiolate formation and proton release from the enzyme are not strictly coupled, because proton release (as well as k_{cat}) was found to be ≈4 times slower than GSH thiolate formation in an unbuffered system. Solvent kinetic isotope effect measurements demonstrated a 2-fold decrease in the rate constant (k_2) for thiolate formation and k_{cat} (in the reaction with 1-chloro-2,4-dinitrobenzene) for both unactivated and activated MGST1. This indicates that thiolate formation contributes to k_{cat} for the activated enzyme, as suggested previously for unactivated MGST1. The stoichiometry of thiolate formation, proton release, and burst kinetics suggested utilization of one GSH molecule per enzyme trimer.

Glutathione transferases (GSTs,[1] EC 2.5.1.18) catalyze the conjugation of the tripeptide glutathione (GSH) to a vast variety of electrophilic compounds, of both xenobiotic and endogenous origin. These enzymes are found in most aerobic organisms and probably constitute the single most important protection system against electrophile damage in the cell (*1*). The soluble GST superfamily consists of at least nine subfamilies, which in turn can consist of several isoenzymes (*2*−*5*). The membrane-bound GSTs are grouped into the recently defined MAPEG (membrane-associated proteins in eicosanoid and GSH metabolism) superfamily, whose members include microsomal GSH transferase 1 (MGST1), MGST2, MGST3, leukotriene C_4 synthase, prostaglandin E synthase, and 5-lipoxygenase-activating protein (*6*). The MAPEG superfamily thus consists of enzymes with broad second substrate specificity, i.e., MGST1, and enzymes that are more specific (leukotriene C_4 synthase and prostaglandin E synthase).

MGST1 is a trimeric enzyme that can be activated, up to 30-fold, by sulfhydryl reagents and other treatments including proteolysis (*7*−*11*). Activation of MGST1 has been observed in vivo (*12*−*16*). The target of activation is usually covalent modification of a single cysteine in the monomer, although proteolytic cleavage (e.g., at lysine-41) also results in activation. Because MGST1 does not respond to traditional transcriptional activators of GSTs, it is thought that activation could be an alternative rapid response to an increased burden of electrophiles in the cell.

We have previously shown that unactivated MGST1 displays several interesting mechanistic features (*17*): (i) GSH binding and ionization to form the nucleophilic thiolate anion is a very slow process in contrast to the cytosolic enzymes (*18*−*21*); (ii) the reaction of the thiolate with the electrophilic substrate occurs by a rapid two-step mechanism with a strong dependence on chemical reactivity. When the second substrate is sufficiently reactive, the overall turnover of MGST1 is limited by the rate of thiolate anion formation (*22*, *23*); (iii) the stoichiometry of GSH thiolate formed, together with burst kinetics, suggested that only one GS$^-$ is bound per trimer of enzyme; and (iv) the kinetics of thiolate

† Supported by the Swedish Cancer Society and the Swedish National Board for Laboratory Animals. Funds from Karolinska Institutet and Grants R01 GM30910 and P30 ES00267 from the National Institutes of Health.

* To whom correspondence should be addressed. Tel: +46 852 487 574. Fax: +46 834 3849. E-mail: ralf.morgenstern@imm.ki.se.

‡ Karolinska Institutet.

§ Vanderbilt University.

[1] Abbreviations: GSH, glutathione; GSO_3^-; glutathione sulfonate; GST, glutathione transferase; MGST, microsomal glutathione transferase; CDNB, 1-chloro-2,4-dinitrobenzene; CNAP, 4-chloro-3-nitroacetophenone; CNBAM, 4-chloro-3-nitrobenzamide; TNB, 1,3,5-trinitrobenzene; NEM, *N*-ethylmaleimide; EDTA, ethylenediamine tetraacetic acid.

10.1021/bi0492511 CCC: $27.50
Published on Web 06/17/2004

anion formation is enhanced by activation of the enzyme with sulfhydryl reagents.

To fully characterize the mechanistic consequences of activation, we present a detailed characterization of the *N*-ethylmaleimide (NEM)-activated MGST1 with respect to the steady-state kinetics, the kinetics of thiolate formation, and chemical catalysis. In addition, solvent kinetic isotope effects on both the unactivated and activated enzyme suggest that thiolate formation and k_{cat} are sensitive in a similar manner, supporting previous suggestions that thiolate anion formation limits turnover.

EXPERIMENTAL PROCEDURES

Chemicals. 1-Chloro-2,4-dinitrobenzene (CDNB) was obtained from Merck Co. (Darmstadt, Germany). 4-Chloro-3-nitroacetophenone (CNAP) was from Aldrich−Chemie (Steinheim, Germany). 4-Chloro-3-nitrobenzamide (CNBAM) was from Alfred Bader Library of Rare Chemicals, Division of Aldrich Chemical Co. (Milwaukee, WI). GSH, glutathione sulfonate (GSO_3^-), deuterium oxide (99.9% D), and NEM were from Sigma Chemical Co. (St. Louis, MO). Bromocresol purple was from (Fluka Chemie AG, Buchs, Switzerland). 1,3,5-Trinitrobenzene (TNB) was a generous gift from Nobel-Chemistry (Karlskoga, Sweden). All other chemicals were of reagent grade and obtained from common commercial sources.

Enzyme Preparation. MGST1 was purified from rat liver as previously described (*24*), with the exception that 0.2% Triton X-100 was used during the final purification step to reduce the interference from Triton X-100 absorbance when analyzing spectral changes at lower wavelengths. Preparation of the enzyme for stopped-flow experiments involved buffer exchange and GSH removal on 10 DG gel-filtration columns (Bio-Rad Laboratories) according to the instructions of the manufacturer. Buffers used were 0.1 M potassium phosphate (pH 7.0) containing 20% glycerol, 0.1 mM ethylenediamine tetraacetic acid (EDTA) and 0.2% Triton X-100 (buffer A); 80 mM NaCl, 0.08 mM EDTA, 20% glycerol, 0.2% Triton X-100, and 10 μM bromocresol purple (pH 7.0) (buffer B); and buffer C, which is identical in composition to buffer A except using D_2O as a solvent. Buffer C was prepared as follows: glycerol (87%) was dissolved in D_2O (1:1), and the solvent was evaporated. This procedure was repeated three times. The other components were then added. The pD was set on a standard pH electrode by adjusting the pH-meter reading according to the following formula: pD = (pH-meter reading) + 0.4 (*25*). Activation of MGST1 was accomplished by adding NEM (5 mM final concentration) to the enzyme, on ice, in a purification buffer. After approximately 10 min, the sample was run on the gel-filtration column. The activated enzyme was kept on ice at all times and was prepared prior to the experiment on the same day.

Stopped-Flow Experiments. Applied Photophysics stopped-flow instruments equipped with either one or two monochromators were used for all experiments. Between 50 and 100 μL from each of two syringes was rapidly mixed in the 10-mm path length cell if not otherwise indicated, and the signal was recorded. In general, 3−6-trace averages were used to fit theoretical expressions describing either single or double exponential or, where appropriate, a single exponential followed by a steady state. All experiments were performed at 4−6 °C. All concentrations given below are the resulting final concentrations in the observation cell. The enzyme concentration is expressed as the concentration of subunits.

GSH Binding, Thiolate Anion Formation, and GSH Release. Enzyme (10−50 μM) in buffer A or C was rapidly mixed with the same buffer containing 0.1−100 mM GSH. The appearance of the absorbance at 239 nm was followed and fitted to a double exponential with the software provided (ϵ_{239} = 5000 M^{-1} cm^{-1}). An optical path length of 10 mm was used except with 25−100 mM GSH, where a 2-mm cell was employed to allow for the high-background absorbance of GSH. When measuring the formation of the Meisenheimer or σ complex (ϵ_{450} = 27 000 M^{-1} cm^{-1}), which is stabilized by MGST1, the enzyme (in buffer A or B) preincubated with 0.4 mM TNB was rapidly mixed with GSH in the same concentration range as above (*26*).

GSH release was followed at 239 nm by mixing 15−30 μM enzyme containing 1 mM GSH with 10, 20, or 30 mM GSO_3^- at pH/D 7.0. The absorbance decrease was recorded on a Philips PU8720 spectrophotometer or on the stopped-flow spectrophotometer when measuring the unactivated or activated enzyme, respectively. The data were fitted to a single exponential by Graphpad Prism 3 or with the program provided with the stopped-flow spectrophotometer and are representative of at least three separate measurements.

Proton Release. Activated enzyme (20−40 μM) in buffer B (pH 7.0) was rapidly mixed with the same buffer containing 0.2−100 mM GSH (pH 7.0). The change in pH was followed with an absorbance decrease in bromocresol purple at 588 nm and was fitted to a double exponential. Independent experiments to obtain the stoichiometry of proton release were performed where 1 mM NaOH was used to titrate back to the original absorbance obtained just after GSH addition. In the potentiometric measurements, the enzyme (90−120 μM) in buffer B was mixed with 1 mM GSH. Again, 1 mM NaOH was used to titrate back to the original pH. No interference by CO_2 within the experimental time was detected. The activated enzyme is unstable in the absence of GSH; therefore, to prevent precipitation, the enzyme was kept on ice or at ≈5 °C at all times. In addition, the amount of active enzyme that correlated to the amount of H^+ released was investigated in a separate experiment. Immediately after measuring the amount of protons released, as described above, the same sample was checked for the amount of active sites in the stopped-flow spectrophotometer, using CDNB as described below.

Presteady-State Kinetics. Burst kinetics were investigated using unactivated or activated enzyme in buffer A or C containing 0.5 mM GSH. The enzyme sample was rapidly mixed with the buffer containing CDNB (ϵ_{340} = 9600 M^{-1} cm^{-1}), CNAP (ϵ_{297} = 11 900 M^{-1} cm^{-1}) or CNBAM (ϵ_{370} = 3100 M^{-1} cm^{-1}), and the burst of product formation was recorded at the indicated wavelength. The burst was fitted to a single exponential or a single exponential followed by a steady state.

Steady-State Kinetics. Steady-state kinetic parameters for MGST1 were determined on a Philips PU8720 spectrophotometer at an assay temperature of 5 °C in buffer A, B, or C. GSH was varied between 0.1 and 100 mM at 0.5 mM

CDNB. CDNB was varied between 0.001 and 0.5 mM at 10 mM GSH (*27*). At least triplicate determinations were performed at each concentration. Data were fitted to the Michaelis−Menten equation yielding the kinetic parameters k_{cat} and K_M. The dependence of enzyme activity on phosphate was investigated by the increased addition of phosphate to the enzyme in buffer B after which the activity was measured with saturating concentrations of GSH (5−25 mM)/CDNB (0.5 mM).

Regression Analysis. All linear and nonlinear regression analyses were performed with the software provided with the stopped-flow spectrophotometer or alternatively using Graphpad Prism 3 (Graphpad Software Inc.).

RESULTS

Thiolate Formation with the Activated Enzyme. An essential aspect of GST catalysis involves the formation and stabilization of a reactive GSH thiolate in the active site (*28*). Formation of the thiolate can be monitored either directly at 239 nm or by a Meisenheimer dead-end complex, rapidly formed in the reaction between enzyme-bound thiolate and TNB at 450 nm. The fate of the GSH proton, which may or may not be released from the enzyme into solution, can be monitored by a pH indicator. Figure 1 shows representative traces obtained when rapidly mixing NEM-activated MGST1 with 1 mM GSH, demonstrating that GSH thiolate and Meisenheimer complex formations display identical kinetics. Proton release however showed a different behavior.

Previous results suggested that binding of GSH to the unactivated enzyme is best described by a two-step mechanism, consisting of an initial rapid equilibrium-binding step followed by a slower formation of thiolate according to Scheme 1. Thiolate formation with the activated enzyme is enhanced and displays more complex biphasic kinetics. The dependence of k_{obs} on [GSH] for the rapid phase of thiolate formation exhibits a saturation behavior (Figure 2) and suggests a two-step process similar to that observed with the unactivated enzyme (*29*). The data were fit to a hyperbolic function (eq 1) to obtain the dissociation constant for GSH in the initial complex (K_D^{GSH}) and the rate constants for ionization and reprotonation/release of GSH (k_2 and k_{-2}) as shown in Table 1. As indicated in Figure 2, the rates of σ-complex formation with TNB accurately follow the rates of thiolate formation. The second, slower phase of thiolate formation (○, parts A and B of Figure 2) occurs at a rate constant that is much smaller than k_{cat} and probably does not contribute to catalysis.

$$k_{obs} = k_{-2} + \frac{k_2[\mathrm{GSH}]}{K_D^{GSH} + [\mathrm{GSH}]} \quad (1)$$

Proton release shows a more complex behavior displaying a much slower rate that is clearly not kinetically associated with thiolate formation (Figure 2C). An increase of k_{obs} is noted at low GSH concentrations, which plateaus early, around 1 mM with a rate of $\approx$1 s^{-1}. Above this concentration, the observed rate of proton release shows a negative dependence on [GSH]. Independent titrations with a pH electrode suggested that one H^+ is released per trimer of enzyme, the same as for unactivated MGST1 (not shown).

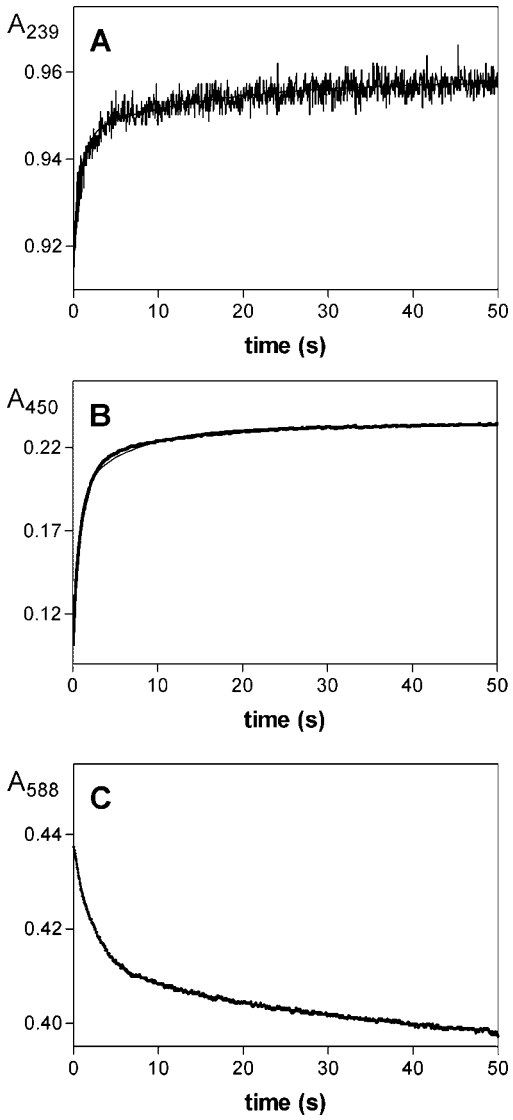

FIGURE 1: Thiolate formation (E•GS$^-$), σ-complex stabilization, and proton release of NEM-activated MGST1. (A) Increase in absorbance at 239 nm upon mixing activated MGST1 (30 μM) with 1 mM GSH. (B) Increase in absorbance at 450 nm because of σ-complex stabilization on activated MGST1 (17 μM) mixed with 1 mM GSH. (C) Loss of absorbance of bromocresol purple at 588 nm because of proton release, caused by mixing activated MGST1 with GSH (1 mM). The respective traces are fitted to double-exponential functions (—), which yields (A) $k_{obs}^1 = 1.1 \pm 0.03$ s^{-1} and $k_{obs}^2 = 0.07 \pm 0.005$ s^{-1}; (B) $k_{obs}^1 = 1.3 \pm 0.01$ s^{-1} and $k_{obs}^2 = 0.14 \pm 0.002$ s^{-1}; and (C) $k_{obs}^1 = 0.43 \pm 0.004$ s^{-1} and $k_{obs}^2 = 0.03 \pm 0.001$ s^{-1}.

Scheme 1

$$E + GSH \underset{}{\overset{K_D^{GSH}}{\rightleftharpoons}} E \bullet GSH \underset{k_{-2}}{\overset{k_2}{\rightleftharpoons}} E \bullet GS^- + H^+$$

A plot of the relative amplitudes obtained from the regression fit is shown in Figure 3 (relative to the measured protein concentration). From Figure 3A, it is apparent that the faster phase dominates at high GSH, while the slower phase is equal or slightly more prominent at the other extreme (Figure 3B), with an intersection point at approximately 0.5 mM.

To obtain a precise value for the off-rate (k_{-2}) of GS$^-$, which is not well-determined by the numerical fits to the stopped-flow-binding data (Table 1), the release of GSH was determined by rapidly mixing the E•GS$^-$ complex with a

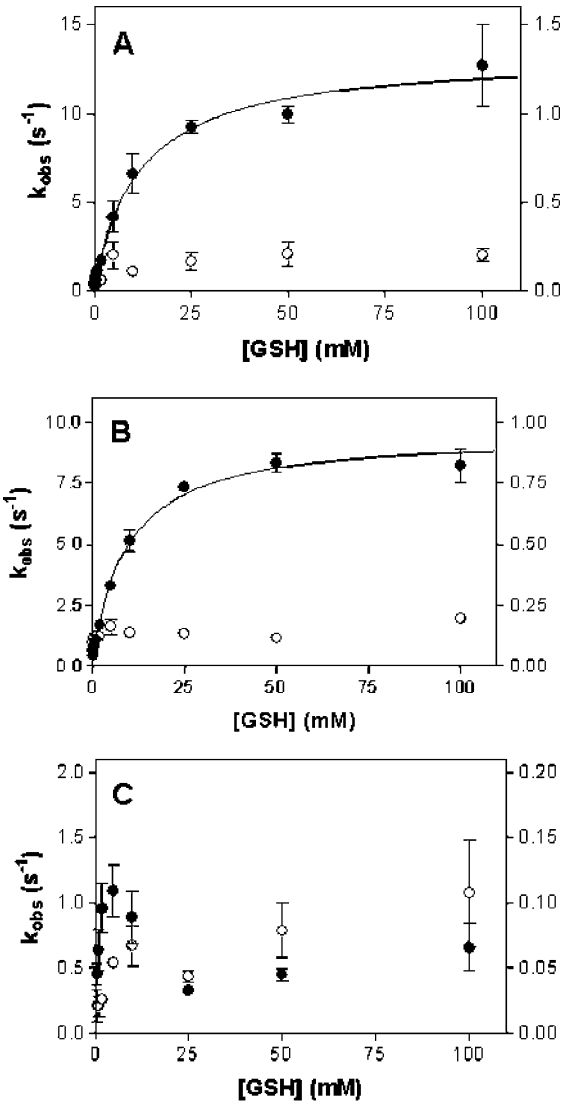

FIGURE 2: Dependence of k_{obs}^1 and k_{obs}^2 on [GSH]. (A) thiolate formation (E•GS$^-$), (B) σ-complex stabilization, and (C) proton release. Note, k_{obs}^1 (●) is plotted on the left y axis and k_{obs}^2 (○) is plotted on the right y axis. The solid lines are best fits of the data to eq 1. Equilibrium constants and rate constants from fits are listed in Table 1.

Table 1: Kinetic Constants of Thiolate Anion Formation with Activated MGST1 at 5 °C

experiment	K_D (mM)	k_2 (s^{-1})	k_{-2} (s^{-1})
thiolate formation[a]	11.7 ± 3.1	13.2 ± 0.9	0.2 ± 0.4
σ-complex formation[a]	9.4 ± 1.2	9.3 ± 0.3	0.3 ± 0.2
GS$^-$ release[b]			0.016 ± 0.000 05

[a] Kinetic constants obtained from the fit of the experimental data (Figure 2) to eq 1. [b] Obtained from the fit of the experimental data (Figure 4) to a single-exponential function.

large excess of inhibitor GSO_3^- ($K_D \approx 20$ μM; ref *30*). The release, illustrated in Figure 4, follows a single exponential that yields a well-defined rate constant for the off reaction (Table 1). The magnitude of the rate constant was independent of the inhibitor concentration when [GSO_3^-] ≥ 10 mM. The observed decrease in absorbance could also be the result of a rate-determining protonation of the E•GS$^-$ complex.

Chemical Step: Reaction with the Electrophilic Substrate. Rapid mixing of the E•GS$^-$ complex with CDNB or CNAP (Figure 5) gives rise to a burst of product formation followed

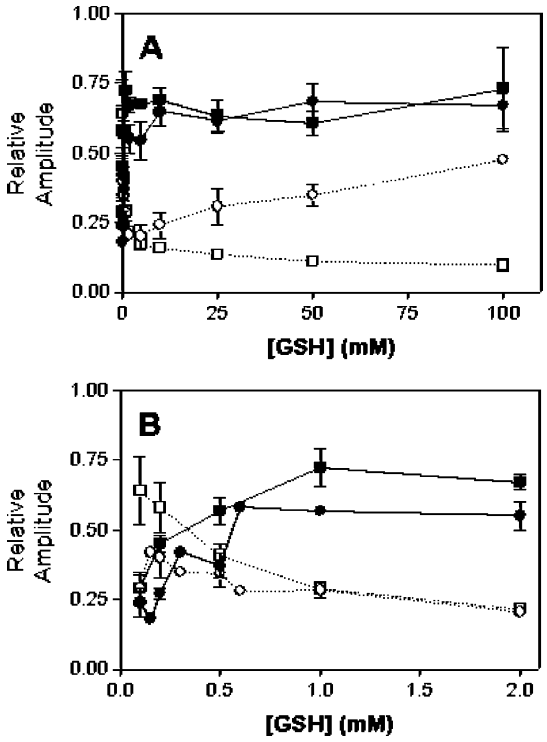

FIGURE 3: (A) Plot of the relative amplitudes of k_{obs}^1 and k_{obs}^2 obtained from fitting experimental data to a double exponential with respect to [GSH]. Normalized with the measured protein concentration. Thiolate formation = k_{obs}^1 (●) and k_{obs}^2 (○), and σ-complex stabilization = k_{obs}^1 (■) and k_{obs}^2 (□). A solid line connects the points of the faster phase, while the dotted line represents the slower phase. (B) Magnification of A, for clarity.

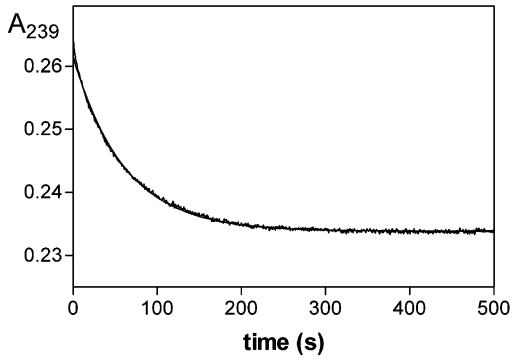

FIGURE 4: Loss of absorbance at 239 nm upon mixing GSO_3^- (20 mM) with the E•GS$^-$ complex (20 μM, with 1 mM GSH), because of the release of GSH. The experimental trace was fitted to a single-exponential function (solid line), which yields a rate constant of 0.016 ± 0.000 05 s^{-1}.

by a steady state. This behavior is consistent with the rate-limiting formation of the E•GS$^-$ complex after the first turnover of the enzyme with the more reactive substrates CDNB and CNAP. The dependence of k_{obs} on the electrophile concentration is shown in parts C and D of Figure 5.

The less reactive substrate, CNAP, exhibited saturation kinetics for k_4, consistent with a simple two-step mechanism with rapid equilibrium binding, followed by the chemical reaction (Scheme 2) in which $k_{-4} = 0$, to reflect the fact that the reaction is essentially irreversible. No saturation for the interaction with CDNB could be observed with the E•GS$^-$ complex, suggesting that CDNB binds much less tightly. The data were therefore fit to a linear rate expression (eq 2, at low [S] = CDNB or CNAP), which yields the

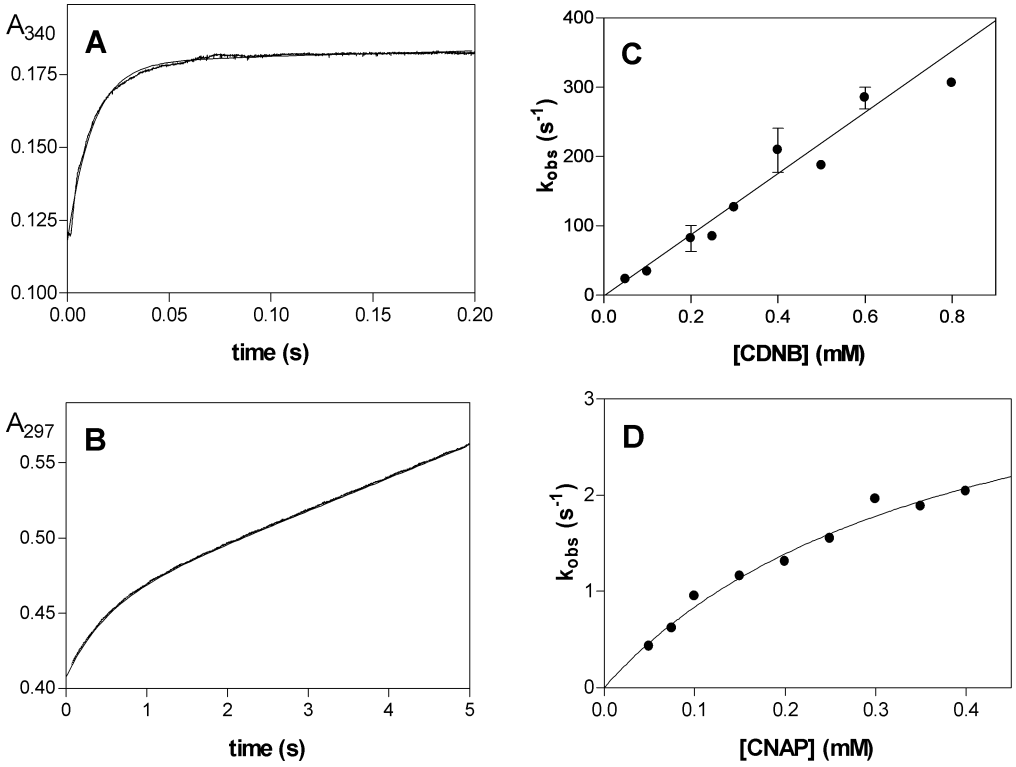

FIGURE 5: Presteady-state kinetics of the reaction of electrophiles with activated E•GS^- complex. (A) Burst of product formation observed at 340 nm upon mixing CDNB (0.2 mM) with E•GS^- (14 μM, containing 0.5 mM GSH). Fit to a single exponential yielded at a rate constant on the burst of 82 ± 0.4 s^{-1}. (B) Burst of product formation followed by a steady-state rate, observed at 297 nm upon mixing CNAP (0.4 mM) with E•GS^- (12 μM, containing 0.5 mM GSH). Fit to a single exponential followed by a steady state yielded a rate constant on the burst of 2.0 ± 0.007 s^{-1}. Dependence of k_{obs} for the burst on [CDNB] (C) or [CNAP] (D). (C) The solid line is a fit of the experimental data to a linear function [eq 2 at low [CDNB], i.e., $k_{obs} = (k_4/K_D^{CDNB})$], which yields the apparent second-order rate constant for the reaction between E•GS^- and CDNB, $k_4/K_D^{CDNB} = 4.4 \pm 0.4 \times 10^5$ M^{-1} s^{-1}. (D) The solid line is a fit of the experimental data to eq 2, which yields the dissociation constant of CNAP ($K_D^{CNAP} = 0.4 \pm 0.1$ mM) and the rate constant for the chemical reaction ($k_4 = 4.1 \pm 0.7$ s^{-1}).

apparent second-order rate constant for the reaction, $k_4/K_D^{CDNB} = (4.4 \pm 0.4) \times 10^5$ M^{-1} s^{-1} (Table 2).

$$k_{obs} = \frac{k_4[S]}{K_D^E + [S]} \quad (2)$$

Solvent Isotope Effects on Steady-State Kinetics and Thiolate Formation. The solvent deuterium isotope effects on the steady-state kinetics are summarized in Table 3. The isotope effects on the unactivated enzyme are approximately 2 for both k_{cat} and k_{cat}/K_M. In general, the solvent isotope effects on the activated enzyme tend to be smaller and in the range of 1.3−2.0. This trend suggests a change in the isotopically sensitive step.

The influence of solvent isotope on the steps leading to thiolate formation is shown in Table 4. The amplitudes of thiolate formation were not altered at pH/pD. Furthermore, $k_{cat}/K_{m(CDNB)}$ was insensitive to pH/pD between 6.5 and 7.5 (not shown), demonstrating that pK_a alterations did not influence the results. The isotope effects on the rate constants for the slow step k_2 and k_{-2} (Scheme 1) are normal except that for k_{-2} with the activated enzyme, where it is inverse $^Hk_{-2}/^Dk_{-2} = 0.44$. The equilibrium isotope effect for the slow step $^HK/^DK = {}^H(k_2/k_{-2})/{}^D(k_2/k_{-2})$ is 2.2 for the unactivated enzyme and 3.5 for the activated enzyme. This behavior suggests that the extent or the identity of the isotopically sensitive proton transfer in the transition state for thiolate formation is altered by the chemical modification of C49. The observation of similar normal isotope effects for thiolate formation and k_{cat} in the steady state is consistent with the conclusion that this step contributes to k_{cat}.

Kinetic Solvent Isotope Effect on the Chemical Reaction. The effects of solvent isotope on the chemical reaction of the enzyme-bound thiolate and three electrophilic substrates are given in Table 5. In contrast to the normal solvent deuterium isotope effects observed on thiolate formation and the steady-state kinetics, the chemical reaction exhibits an inverse isotope effect of about 0.6−0.8. Within the errors of the measurements, there are no significant differences in the isotope effects between the unactivated and activated enzyme. It is nevertheless clear that electrophile binding and the chemical reaction do not contribute to the solvent isotope effect observed in steady-state turnover particularly with reactive second substrates such as CDNB. The magnitude of the inverse isotope effect is close to that expected for a solvated or hydrogen-bonded thiolate as the nucleophile (*31*).

DISCUSSION

Thiolate Formation and Catalysis by the Activated Enzyme. The kinetics of thiolate anion formation with activated MGST1 is biphasic, where the faster, dominant phase, can be described by initial rapid equilibrium binding of GSH followed by a slower formation of the thiolate (Scheme 1 and Table 1). The overall $K_D^{GS^-}$ can be calculated from the

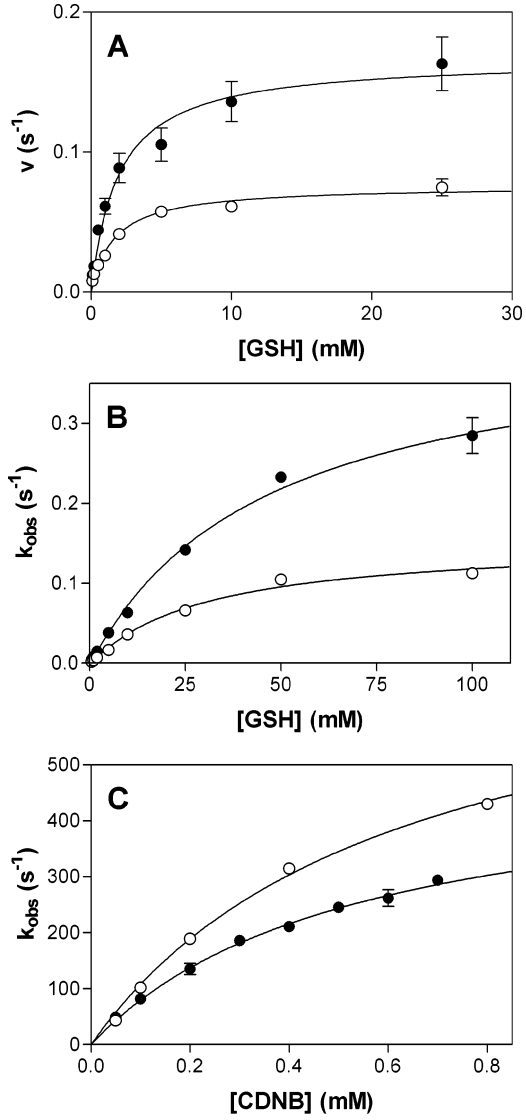

FIGURE 6: Effect of D_2O on various kinetic parameters with unactivated MGST1, H_2O (●) and D_2O (○). (A) Plot of initial rate kinetics on varying GSH with constant CDNB (0.5 mM), normalized with the enzyme concentration. Kinetic constants from the fit to a Michaelis−Menten expression are found in Table 3. (B) Thiolate anion formation at 239 nm. Kinetic constants from the fit to eq 1 are found in Table 4. (C) Burst kinetics of the reaction of E•GS$^-$ with CDNB. Kinetic constants from the fit to eq 2 are found in Table 5.

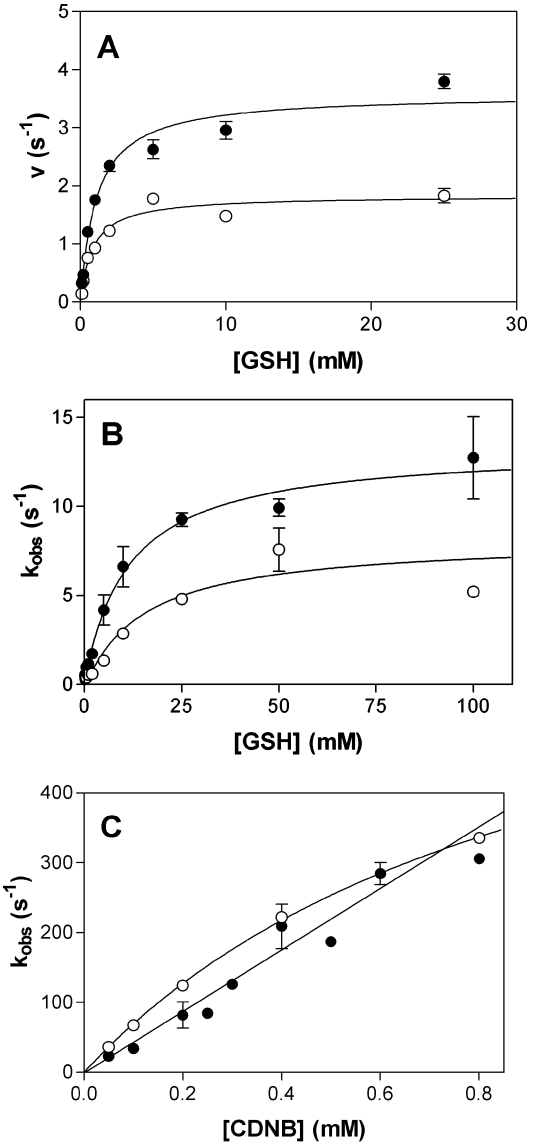

FIGURE 7: Effect of D_2O on various kinetic parameters for NEM-activated MGST1, H_2O (●) and D_2O (○). (A) Plot of initial rate kinetics on varying GSH with constant CDNB (0.5 mM), normalized with the enzyme concentration. Kinetic constants from the fit to a Michaelis−Menten expression are found in Table 3. (B) Thiolate anion formation at 239 nm. Kinetic constants from the fit of the fast phase to eq 1 are found in Table 4. (C) Burst kinetics of the reaction of E•GS$^-$ with CDNB. Kinetic constants from a linear fit (●) or the fit to eq 2 (○) are found in Table 5.

constants k_2, k_{-2}, and K_D^{GSH} and was found to be 14 ± 4 μM, which indicates high affinity of GSH for activated MGST1. This value is in good agreement with that determined earlier by equilibrium dialysis (22 ± 5 μM) (*30*).

Figure 3 shows the relative amplitudes obtained when fitting data for thiolate formation to a double-exponential function. The amplitude of the slow phase is equal to or larger than the fast phase at low GSH. At high GSH > 1 mM, the fast phase dominates and the slow phase is less apparent. There is a difference between the amplitude behavior for thiolate and σ-complex formations at high GSH, probably because of the fact that the slow phase makes a minor contribution and is therefore more difficult to determine with good precision at 239 nm. When measuring σ-complex formation, higher extinction/sensitivity is obtained at 450 nm, where neither GS$^-$, the protein, nor Triton X-100 absorbs. The basis for the biphasic behavior of activated MGST1 is not known, but it can be speculated that the GSH-free enzyme can adopt a different conformation that is less active and that this conformation is reversed upon the initial interaction with GSH. In any case, the slow phases cannot contribute to steady-state turnover because they are much lower than k_{cat}.

Scheme 2

$$E \bullet GS^- + S \underset{}{\overset{K_D^E}{\rightleftharpoons}} E \bullet GS^- \bullet S \xrightarrow{k_4} E \bullet P + Cl^-$$

Table 2: Kinetic Constants for the Reaction of CDNB and CNAP with the E•GS$^-$ Complex of Activated MGST1 at 5 °C

substrate	K_D^E (mM)	k_4 (s^{-1})	k_4/K_D^E (M^{-1} s^{-1})
CDNB			$(4.4 \pm 0.4) \times 10^5$
CNAP	0.4 ± 0.1	4.1 ± 0.7	$(1.0 \pm 0.3) \times 10^4$

Table 3: Steady-State Kinetic Constants of MGST1 in the Reaction between GSH and CDNB, in H_2O or D_2O Obtained at 5 °C

	unactivated MGST1			activated MGST1		
substrate/solvent	k_{cat} (s^{-1})	K_M (mM)	k_{cat}/K_M (M^{-1} s^{-1})	k_{cat} (s^{-1})	K_M (mM)	k_{cat}/K_M (M^{-1} s^{-1})
GSH/H_2O	0.17 ± 0.01	2.0 ± 0.4	85 ± 18	3.6 ± 0.1	1.1 ± 0.1	(3.3 ± 0.3) × 10^3
GSH/D_2O	0.08 ± 0.003	1.6 ± 0.2	50 ± 7	1.8 ± 0.1	0.8 ± 0.1	(2.3 ± 0.3) × 10^3
$^{H}k/^{D}k$	2.1 ± 0.1		1.7 ± 0.3	2.0 ± 0.1		1.4 ± 0.2
CDNB/H_2O	0.14 ± 0.005	(11 ± 2) × 10^{-3}	(13 ± 2) × 10^3	2.8 ± 0.1	(5 ± 1) × 10^{-3}	(5.6 ± 1.1) × 10^5
CDNB/D_2O	0.07 ± 0.003	(19 ± 4) × 10^{-3}	(4 ± 1) × 10^3	2.2 ± 0.1	(5 ± 1) × 10^{-3}	(4.4 ± 0.9) × 10^5
$^{H}k/^{D}k$	2.0 ± 0.1		3.2 ± 0.8	1.3 ± 0.1		1.3 ± 0.3

Table 4: Kinetic Constants of Thiolate Anion Formation of MGST1, in H_2O or D_2O Obtained at 5 °C

	unactivated MGST1			activated MGST1		
substrate/solvent	k_2 (s^{-1})	K_D (mM)	k_{-2} (s^{-1})	k_2 (s^{-1})	K_D (mM)	k_{-2} (s^{-1})
GSH/H_2O	0.42 ± 0.03[a]	47 ± 7[a]	(6 ± 0.3) × 10^{-4} [a]	13.2 ± 0.9	11.7 ± 3.1	0.016 ± 0.000 05
GSH/D_2O	0.16 ± 0.003	30 ± 6	(5 ± 0.8) × 10^{-4}	8.4 ± 1.4	15 ± 10	0.036 ± 0.0006
$^{H}k/^{D}k$	2.6 ± 0.2		1.2 ± 0.2	1.6 ± 0.3		0.44 ± 0.01

[a] From ref *17*.

Table 5: Kinetic Constants and Isotope Effects for the Reaction between Electrophilic Substrates and the E•GS^- Complex, in H_2O or D_2O Obtained at 5 °C

	unactivated MGST1			activated MGST1		
substrate/solvent	k_4 (s^{-1})	K_D (mM)	k_4/K_D^E (M^{-1} s^{-1})	k_4 (s^{-1})	K_D (mM)	k_4/K_D^E (M^{-1} s^{-1})
CDNB/H_2O	510 ± 40[a]	0.5 ± 0.1[a]	(9.6 ± 1.6) × 10^5			(4.4 ± 0.4) × 10^5[b]
CDNB/D_2O	770 ± 60	0.6 ± 0.1	(1.3 ± 0.2) × 10^6	750 ± 35	0.97 ± 0.07	(7.7 ± 0.7) × 10^5
$^{H}k/^{D}k$	0.66 ± 0.05		0.7 ± 0.1			0.57 ± 0.05
CNAP/H_2O	15 ± 6[a]	1.1 ± 0.6[a]	(1.4 ± 0.9) × 10^4	4.1 ± 0.7	0.4 ± 0.1	(1.0 ± 0.3) × 10^4
CNAP/D_2O	13 ± 3	0.6 ± 0.2	(2.3 ± 0.8) × 10^4	6.8 ± 0.9	0.4 ± 0.1	(1.7 ± 0.5) × 10^4
$^{H}k/^{D}k$	1.2 ± 0.4		0.6 ± 0.4	0.6 ± 0.1		0.6 ± 0.2
CNBAM/H_2O	1.0 ± 0.1[a]	0.6 ± 0.1[a]	(1.8 ± 0.3) × 10^3			
CNBAM/D_2O	1.3 ± 0.1	0.2 ± 0.04	(5.7 ± 1.1) × 10^3			
$^{H}k/^{D}k$	0.77 ± 0.08		0.3 ± 0.2			

[a] From ref *17*. [b] Apparent value, from linear regression in Figure 5C.

One intriguing observation comes from the proton-release experiments. At low GSH, the observed rate of proton release appears to follow the rate of thiolate anion formation. However, at higher GSH concentrations, proton release becomes dissociated from and much slower (Figure 2C) than the rapid rates of thiolate formation (parts A and B of Figure 2). It should be pointed out that thiolate anion formation is measured in phosphate buffer, whereas proton release of course has to be measured in an unbuffered salt solution. Whereas thiolate anion formation was independent of the buffer composition (measured using TNB and "buffer" B in the stopped flow (k_2 = 7.3 ± 0.3 s^{-1} and K_D^{GSH} = 17 ± 3 mM; not shown), we could show that proton release is not independent. The slow proton release can actually determine k_{cat} in the unbuffered system because the turnover number was much lower (k_{cat} = 0.71 ± 0.06 s^{-1} and K_M = 1.11 ± 0.35 mM) compared to k_{cat} in phosphate buffer at the same pH. The steady-state rate was shown, in separate experiments, to be strongly dependent on phosphate addition, increasing by a factor of 4. A high salt concentration (0.08 M NaCl) was also shown to have a slight inhibitory effect (≈30%). It is possible that phosphate ($H_2PO_4^-$/HPO_4^{2-} ≈ 50:50 at pH 7) functions as a proton acceptor, but its specific role and the mechanism are a subject of future studies. The complex rate concentration behavior of proton release could perhaps stem from the combined effects of raising ionic strength and buffer capacity when increasing the concentration of GSH as high as 100 mM. In summary, thiolate anion formation kinetics for activated MGST1 is consistent with an important role in the overall rate behavior. However, it cannot be excluded that proton release is a major contributor (because it appears to be the major rate-limiting step under certain conditions).

The kinetic solvent isotope effects on thiolate formation with the unactivated and activated enzyme are distinct and provide some insight into the differences in the two processes, although the effects are complex (primary, secondary, and medium isotope effects collectively) and cannot be assigned to any particular proton site (*32*, *33*). Kinetic solvent isotope effects ($^{H}k/^{D}k$) on the forward (k_2) and reverse (k_{-2}) reactions can be cast in terms of the fractionation factors of the transition state (ϕ^T), reactant (ϕ^R), and product (ϕ^P) and the extent of proton transfer (α) in the transition state (eq 3). The equilibrium isotope effect $^{H}K/^{D}K$ (eq 4) combined with the kinetic isotope effect can be used to estimate the extent of proton transfer. If proton transfer is complete in the transition state (α = 1), then the equilibrium and kinetic isotope effects are the same.

$$^{H}k/^{D}k = \phi^R/\phi^T = (\phi^R/\phi^P)^{\alpha} \quad (3)$$

$$^{H}K/^{D}K = {}^{H}(k_2/k_{-2})/{}^{D}(k_2/k_{-2}) = (\phi^R/\phi^P) \quad (4)$$

For an unactivated enzyme, the kinetic and equilibrium effects are nearly the same $^{H}k_2/^{D}k_2$ = 2.6 ± 0.2 ≈ $^{H}K/^{D}K$ = 2.2 ± 0.3, so that $\alpha \approx 1$ (1.2 ± 0.4 is the calculated value).

A similar analysis of the isotope effect on k_{-2}, ${}^{H}k_{-2}/{}^{D}k_{-2} = 1.2 \pm 0.2$, is also consistent with $\alpha \approx 1$. Thus, the proton transfer(s) in the isotope-sensitive step in thiolate formation (presumably a conformational change) appears to be essentially complete in the transition state.

In contrast, analysis of the activated enzyme, where the equilibrium and kinetic solvent isotope effects are clearly different, reveals a much smaller value for $\alpha = 0.4 \pm 0.2$, as obtained from the isotope effect on k_2. In addition, the inverse isotope effect on k_{-2}, ${}^{H}k_{-2}/{}^{D}k_{-2} = 0.44 \pm 0.01$, can be recapitulated from the equilibrium effect and α such that $(\phi^{P}/\phi^{R})^{1-\alpha} = (0.28)^{0.6} = 0.47$. Clearly, in the activated enzyme, the kinetically relevant proton(s) is in flight in the transition state. An early transition state is consistent with the possibility that the activated enzyme catalyzes the deprotonation of GSH.

The above analysis of course does not reveal the exact nature of the isotope-sensitive step, which could in principle involve proton transfer from the thiol or crucial changes in hydrogen-bonding patterns in a conformational transition. Nevertheless, it is clear that the mechanism of thiolate anion formation is substantially changed in the activated enzyme and that, overall, these observations are consistent with the notion that thiolate formation contributes substantially to k_{cat}. Because there is a difference in the isotope sensitivity between the activated and unactivated enzyme with respect to thiolate formation that is not seen in k_{cat}, it is possible that other steps in the mechanism, e.g., proton or product release, could also be affected. Preliminary studies on the interaction of the product with MGST1 indeed suggest additional slow isomerizations of this enzyme.

Electrophile Binding and Chemical Catalysis. The reaction of the NEM-activated E•GS^{-} complex with CDNB is a rapid process (Figure 5A). The plot of the observed rate constant against the CDNB concentration could not be fitted to yield a dissociation constant for the E•GS^{-}•CDNB complex, which indicates that the activated enzyme displays a lower affinity for CDNB compared to unactivated MGST1. The reaction with CNAP on the other hand displayed saturation. The rate constant for the chemical reaction, $k_4 \approx 4\ s^{-1}$, suggests that this step is slower than the maximum rate of thiolate anion formation of the activated enzyme. In fact, CNAP only displays an increased turnover rate of ≈7 with the activated enzyme, compared to a theoretical maximum of 30-fold (increased rate of thiolate formation). Further, the dissociation constant, $K_D^{CNAP} \approx 0.4$ mM, is very similar to the observed $K_M^{CNAP} \approx 0.49$ mM, which is expected when the reactivity of the second substrate is lowered and the chemical reaction contributes to the rate-limiting step in turnover (*23*). The ratio of the values of k_4/K_D^E for CDNB and CNAP (ratio ≈ 44) corresponds well to the ratio for the nonenzymatic reaction (ratio ≈ 50). This confirms that the chemical reaction rates obtained with activated MGST1 are strongly dependent on the electrophilic nature of the second substrate (*23*).

Comparison of Activated and Unactivated MGST. The previous investigation on unactivated MGST1 suggested a mechanism that consisted of slow GSH thiolate formation and rapid chemistry, with the former contributing to the rate-limiting step when the second substrate is reactive. This short outline of the enzyme mechanism was also found to be applicable to the activated enzyme with a few important differences as discussed below.

Thiolate anion formation is greatly enhanced in the activated enzyme as depicted by comparison of the rate constants, ${}^{act}k_2/{}^{unact}k_2 \approx 30$. This enhancement is also reflected in k_{cat} of reactive substrates, such as CDNB (${}^{act}k_{cat}/{}^{unact}k_{cat} \approx 20$). When comparing the apparent specificity, at infinitely dilute GSH, with the unactivated enzyme, ${}^{act}(k_2/K_D^{GSH})/{}^{unact}(k_2/K_D^{GSH}) \approx 130$, the increased efficiency for utilization of GSH is even more apparent, stemming, for the most part, from an apparent increase in the affinity for GSH.

The increased rate of thiolate formation in the activated enzyme does not permit a detailed analysis of the burst kinetics with electrophiles of low chemical reactivity. Nevertheless, comparisons can be made with the more reactive CDNB and CNAP. The apparent specificity (k_4/K_D^E) of the activated enzyme for these substrates very closely resembles the values obtained for the unactivated enzyme. This suggests that activated MGST1 is largely similar to the unactivated enzyme with respect to nucleophilic aromatic substitution catalysis. However, some differences exist, e.g., the binding affinity of both substrates and the chemical rate constant (k_4) of CNAP, which is 3−4-fold lower than the rate constant with unactivated MGST1. This indicates that NEM modification does cause differences, however small, that can cause changes in the architecture or dynamics of the putative hydrophobic binding site.

Conclusions. These studies show that activation of MGST1 gives rise to a significantly enhanced efficiency for the utilization of GSH, observed in the kinetics of thiolate anion formation, compared to the unactivated enzyme. The interaction with electrophilic second substrates is largely unaltered upon activation, but the binding and orientation of the substrate could be somewhat affected. Moreover, all of the kinetic data suggest a stoichiometry of GSH binding of one molecule per trimer of enzyme.

ACKNOWLEDGMENT

We thank Prof. Peter Brzezinski and co-workers at Stockholm University for usage of the stopped-flow spectrophotometer.

REFERENCES

1. Rinaldi, R., Eliasson, E., Swedmark, S., and Morgenstern, R. (2002) Reactive intermediates and the dynamics of glutathione transferases, *Drug Metab. Dispos. 30*, 1053−1058.
2. Mannervik, B., Awasthi, Y. C., Board, P. G., Hayes, J. D., Diilio, C., Ketterer, B., Listowsky, I., Morgenstern, R., Muramatsu, M., Pearson, W. R., Pickett, C. B., Sato, K., Widersten, M., and Wolf, C. R. (1992) Nomenclature for Human Glutathione Transferases, *Biochem. J. 282*, 305−306.
3. Hayes, J. D., and Strange, R. C. (2000) Glutathione *S*-transferase polymorphisms and their biological consequences, *Pharmacology 61*, 154−166.
4. Armstrong, R. N. (1997) Structure, Catalytic Mechanism, and Evolution of the Glutathione Transferases, *Chem. Res. Toxicol. 10*, 2−18.
5. Board, P. G., Coggan, M., Chelvanayagam, G., Easteal, S., Jermiin, L. S., Schulte, G. K., Danley, D. E., Hoth, L. R., Griffor, M. C., Kamath, A. V., Rosner, M. H., Chrunyk, B. A., Perregaux, D. E., Gabel, C. A., Geoghegan, K. F., and Pandit, J. (2000) Identification, characterization, and crystal structure of the Omega class glutathione transferases, *J. Biol. Chem. 275*, 24798−24806.
6. Jakobsson, P. J., Morgenstern, R., Mancini, J., Ford-Hutchinson, A., and Persson, B. (1999) Common structural features of MAPEG−A widespread superfamily of membrane associated

proteins with highly divergent functions in eicosanoid and glutathione metabolism, *Protein Sci. 8*, 689−692.
7. Aniya, Y. (1989) Activation of liver microsomal glutathione *S*-transferase by heating, *J. Pharmacobio. Dyn. 12*, 235−240.
8. Andersson, C., Söderström, M., and Mannervik, B. (1988) Activation and inhibition of microsomal glutathione transferase from mouse liver, *Biochem. J. 249*, 819−823.
9. Aniya, Y., and Naito, A. (1993) Oxidative Stress-Induced Activation of Microsomal Glutathione *S*-Transferase in Isolated Rat Liver, *Biochem. Pharmacol. 45*, 37−42.
10. Mosialou, E., Andersson, C., Lundqvist, G., Andersson, G., Bergman, T., Jornvall, H., and Morgenstern, R. (1993) Human Liver Microsomal Glutathione Transferase−Substrate Specificity and Important Protein Sites, *FEBS Lett. 315*, 77−80.
11. Svensson, R., Rinaldi, R., Swedmark, S., and Morgenstern, R. (2000) Reactivity of cysteine-49 and its influence on the activation of microsomal glutathione transferase 1: Evidence for subunit interaction, *Biochemistry 39*, 15144−15149.
12. Masukawa, T., and Iwata, H. (1986) Possible regulation mechanism of microsomal glutathione *S*-transferase activity in rat liver, *Biochem. Pharmacol. 35*, 435−438.
13. Botti, B., Moslen, M. T., Trieff, N. M., and Reynolds, E. S. (1982) Transient decrease of liver cytosolic glutathione *S*-transferase activities in rats given 1,2-dibromoethane or CCl4, *Chem.-Biol. Interact. 42*, 259−270.
14. Haenen, G. R. M. M., Vermeulen, N. P. E., Jacintha, N. L., Tsoi, T. T., Ragetli, H. M. N., Timmerman, H., and Bast, A. (1988) Activation of the microsomal glutathione *S*-transferase and reduction of the glutathione dependent protection against lipid peroxidation by acrolein, *Biochem. Pharmacol. 37*, 1933−1938.
15. Ji, Y., and Bennett, B. M. (2003) Activation of microsomal glutathione *S*-transferase by peroxynitrite, *Mol. Pharmacol. 63*, 136−146.
16. Aniya, Y., Kunii, D., and Yamazaki, K. (2000) Oxidative and proteolytic activation of liver microsomal glutathione *S*-transferase (GSTm), *Chem-Biol. Interact. 133*, 144−147.
17. Morgenstern, R., Svensson, R., Bernat, B. A., and Armstrong, R. N. (2001) Kinetic analysis of the slow ionization of glutathione by microsomal glutathione transferase MGST1, *Biochemistry 40*, 3378−3384.
18. Gustafsson, A., Pettersson, P. L., Grehn, L., Jemth, P., and Mannervik, B. (2001) Role of the glutamyl α-carboxylate of the substrate glutathione in the catalytic mechanism of human glutathione transferase A1-1, *Biochemistry 40*, 15835−15845.
19. Caccuri, A. M., Lobello, M., Nuccetelli, M., Nicotra, M., Rossi, P., Antonini, G., Federici, G., and Ricci, G. (1998) Proton Release Upon Glutathione Binding to Glutathione Transferase P1-1−Kinetic Analysis Of a Multistep Glutathione Binding Process, *Biochemistry 37*, 3028−3034.
20. Jemth, P., and Mannervik, B. (1999) Fast product formation and slow product release are important features in a hysteretic reaction mechanism of glutathione transferase T2-2, *Biochemistry 38*, 9982−9991.
21. Caccuri, A. M., Antonini, G., Board, P. G., Parker, M. W., Nicotra, M., Lo Bello, M., Federici, G., and Ricci, G. (1999) Proton release on binding of glutathione to α, μ, and δ class glutathione transferases, *Biochem. J. 344*, 419−425.
22. Chen, W.-J., Graminski, G. F., and Armstrong, R. N. (1988) Dissection of the catalytic mechanism of isozyme 4-4 of glutathione *S*-transferase with alternate substrates, *Biochemistry 27*, 647−654.
23. Morgenstern, R., Lundqvist, G., Hancock, V., and DePierre, J. W. (1988) Studies on the activity and activation of rat liver microsomal glutathione transferase, in particular with a substrate analogue series, *J. Biol. Chem. 263*, 6671−6675.
24. Morgenstern, R., and DePierre, J. W. (1983) Microsomal glutathione transferase, Purification in unactivated form and further characterization of the activation process, substrate specificity, and amino acid composition, *Eur. J. Biochem. 134*, 591−597.
25. Glasoe, P. K., and Long, F. A. (1960) Use of glass electrodes to measure acidities in deuterium oxide, *J. Phys. Chem. 64*, 188−193.
26. Graminski, G. F., Zhang, P., Sesay, M. A., Ammon, H. L., and Armstrong, R. N. (1989) Formation of the 1-(*S*-glutathionyl)-2,4,6-trinitrocyclohexadienate anion at the active site of glutathione *S*-transferase: Evidence for enzymic stabilization of σ-complex intermediates in nucleophilic aromatic substitution reactions, *Biochemistry 28*, 6252−6258.
27. Habig, W. H., Pabst, M. J., and Jakoby, W. B. (1974) Glutathione *S*-transferases. The first enzymatic step in mercapturic acid formation, *J. Biol. Chem. 249*, 7130−7139.
28. Graminski, G. F., Kubo, Y., and Armstrong, R. N. (1989) Spectroscopic and kinetic evidence for the thiolate anion of glutathione at the active site of glutathione *S*-transferase, *Biochemistry 28*, 3562−3568.
29. Fersht, A. (1999) *Structure and Mechanism in Protein Science*, W. H. Freeman & Co., New York.
30. Sun, T.-H., and Morgenstern, R. (1997) Binding of glutathione and an inhibitor to microsomal glutathione transferase, *Biochem. J. 326*, 193−196.
31. Huskey, S. W., Huskey, W. P., and Lu, A. Y. H. (1991) Contributions of Thiolate "Desolvation" to Catalysis by Glutathione *S*-Transferase Isozymes 1-1 and 2-2: Evidence from Kinetic Solvent Isotope Effects, *J. Am. Chem. Soc.* 113, 2283−2290.
32. Parsons, J. F., and Armstrong, R. N. (1996) Proton Configuration in the Ground State and Transition State of a Glutathione Transferase-Catalyzed Reaction Inferred from the Properties of Tetradeca(3-fluorotyrosyl)glutathione Transferase, *J. Am. Chem. Soc. 118*, 2295−2296.
33. Showen, R. L. (1977) in *Isotope Effects on Enzyme-Catalyzed Reactions* (Cleland, W. W., O'Leary, M. H., and Northrop, D. B., Eds.) pp 64−100, University Park Press, Baltimore, MD.

BI0492511